How to cite: *Angew. Chem. Int. Ed.* **2023,** *62,* e202212438
International Edition: doi.org/10.1002/anie.202212438
German Edition: doi.org/10.1002/ange.202212438

Nanocatalysis

Nanoconfinement-Guided Construction of Nanozymes for Determining H_2O_2 Produced by Sonication

Tong Li, Yuting Wang, Wanling Liu, Houguo Fei, Cunlan Guo, and Hui Wei**

Abstract: Nanomaterials with enzyme-like activities, termed as nanozymes, have found wide applications in various fields. It has been a long-term aim to rationally design and synthesize highly active nanozymes and thus to further improve their application performance. Guided by the nanoconfinement effect, we confine cytochrome c (Cyt c) within a mesoporous metal–organic framework (MOF), PCN-222 nanoparticle (NP), forming a protein/MOF hybrid nanozyme, termed as Cyt c@PCN-222 NP. The confined Cyt c exhibits around 3–4-fold higher peroxidase-like activity than free Cyt c. Due to the increase in the activity of Cyt c, the Cyt c@PCN-222 NPs exhibit a quite low limit of detection ($\approx$0.13 μM) towards H_2O_2. Sonication-induced H_2O_2 formation in water by using a lab-quipped ultrasonic cleaner can be sensitively probed, which suggests that H_2O_2-sensitive materials should be carefully handled during the utilization of ultrasonic equipment. We speculate that this nanoconfinement strategy can broaden our synthetic methodology for the rational design of nanozymes.

Introduction

Nanozymes, the functional nanomaterials exhibiting enzyme-mimicking activities, have attracted increasing interest in diverse fields.[1] Nanozymes have been widely used to mimic a series of enzymes, including peroxidase,[2] oxidase,[3] superoxide dismutase,[4] catalase,[5] hydrolase,[6] and so on. Among them, the peroxidase-mimicking nanozymes, catalyzing the peroxidation of a colorimetric or fluorescent substrate, have been successfully employed to detect a variety of targets from small biomolecules and proteins to cells.[7] The biosensing performance of nanozymes is highly dependent on their activity. Therefore, much effort has been devoted to constructing highly active enzyme-mimicking materials.

Confinement of biomolecules, including enzymes, widely exists in cells, which enables biochemical transformation to proceed efficiently. Inspired by nature, a lot of nanomaterials possessing nanoscale pores, cavities, and channels, such as carbon nanotubes,[8] zeolites,[9] and metal–organic frameworks (MOFs),[10] have been employed to confine catalysts. Such a nanoconfinement has achieved delicate control over catalytic reactions.[11] Among these materials, MOFs stand out due to the excellent designability of metal nodes and organic linkers. The pores or channels in MOFs can be finely tuned from microscale to mesoscale, which enables small molecules and macromolecules to be well confined within the pores or channels.[12] A number of natural enzymes and metalloproteins with intrinsic enzyme-mimicking activities have been successfully confined within the pores or channels in mesoporous MOFs for improved catalytic reactions.[13]

Guided by this nanoconfinement effect, we construct a hybrid peroxidase-mimicking protein/MOF nanozyme by confining a peroxidase-mimicking metalloprotein, cytochrome c (Cyt c), within the channels of a PCN-222 (PCN = porous coordination network) nanoparticle (NP). The formed nanozyme is termed as Cyt c@PCN-222 NP (Figure 1a). PCN-222 exhibits a channel size of 3.7 nm,[14] which is expected to encapsulate Cyt c in an efficient manner. In addition, due to the nanoconfinement effect, PCN-222 NPs can increase the peroxidase-mimicking activity of Cyt c. The Cyt c@PCN-222 nanozyme can be employed to sensitively probe the H_2O_2 formation induced by sonication. This nanoconfinement strategy offers an insight into the design and fabrication of highly active nanozymes, which can further find wide applications in the field of molecular sensing.

Results and Discussion

PCN-222 NPs were fabricated according to a reported method.[15] As shown in Figure 1b, the synthesized PCN-222 NPs exhibited a rod-like shape. The length and width of PCN-222 NPs were measured to be 569 ± 57 nm and 93 ± 11 nm, respectively, by the ImageJ software according to the SEM image. Moreover, the XRD pattern of PCN-222 NPs

[*] T. Li, Y. Wang, W. Liu, Prof. Dr. H. Wei
College of Engineering and Applied Sciences, Nanjing National Laboratory of Microstructures, Jiangsu Key Laboratory of Artificial Functional Materials, Nanjing University
Nanjing, Jiangsu 210023 (China)
E-mail: weihui@nju.edu.cn
H. Fei, Prof. Dr. C. Guo
College of Chemistry and Molecular Sciences, Wuhan University
Wuhan, Hubei 430072 (China)
E-mail: cunlanguo@whu.edu.cn
Prof. Dr. H. Wei
State Key Laboratory of Analytical Chemistry for Life Science, School of Chemistry and Chemical Engineering, Chemistry and Biomedicine Innovation Center (ChemBIC), Nanjing University
Nanjing, Jiangsu 210023 (China)

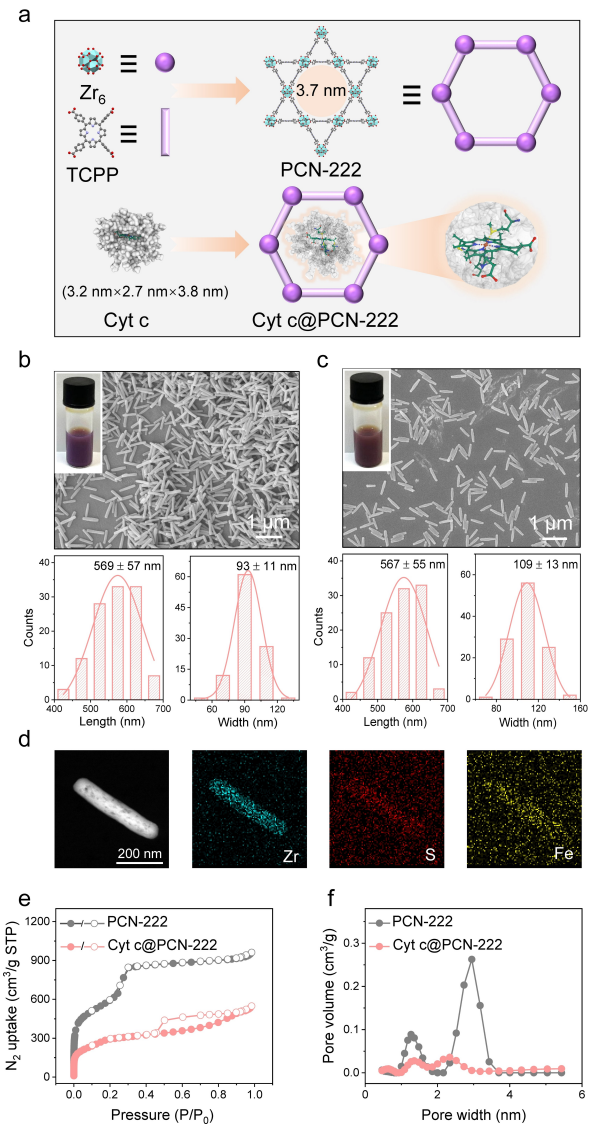

Figure 1. Synthesis and characterization of Cyt c@PCN-222 NPs. a) Schematic illustration of the confinement of Cyt c within the channels of PCN-222 NPs. b), c) SEM images of PCN-222 NPs and Cyt c@PCN-222 NPs, and their corresponding photographs (inset) and size distribution histograms. d) STEM image of Cyt c@PCN-222 and elemental mappings of Zr from PCN-222, and S and Fe from Cyt c. e) N_2 adsorption/desorption isotherms and f) pore size distribution of PCN-222 and Cyt c@PCN-222, respectively.

was also measured, which corresponded well with that of the simulated PCN-222 (Figure S1). For comparison, we also fabricated PCN-222 microparticles, termed as L-PCN-222 MPs, to investigate the effect of the size of PCN-222 on the encapsulation of Cyt c. The fabricated L-PCN-222 MPs also showed a rod-like shape (Figure S2). The length and width of L-PCN-222 MPs were measured to be 4.3 ± 0.6 μm and 0.59 ± 0.06 μm, respectively, which were about 7–8 folds of those of PCN-222 NPs. The XRD pattern of L-PCN-222 MPs was also in accordance with that of simulated PCN-222 (Figure S1). It is known that Cyt c has a characteristic absorption peak at 409 nm. Hence, we measured the standard curve of Cyt c using a microplate reader based on its optical density at 409 nm (Figure S3).

We further incubated PCN-222 NPs and L-PCN-222 MPs with an identical mass concentration of Cyt c solution with or without stirring for varying times. The concentration of free Cyt c in the supernatant was quantified based on the standard curve. As shown in Figure S4, the concentration of unconfined Cyt c in the supernatant after incubation with PCN-222 NPs was much lower than that after incubation with L-PCN-222 MPs, which means that PCN-222 NPs could encapsulate much more Cyt c than L-PCN-222 MPs. The amount of Cyt c in the supernatant reached a plateau after a 3-h incubation with PCN-222 NPs. More than 80 % of Cyt c could be loaded within PCN-222 NPs, while no more than 20 % of Cyt c was encapsulated within L-PCN-222 MPs. This might be because PCN-222 NPs have much more exposed windows, which offer more accessibility for Cyt c into the channels than L-PCN-222 MPs. The shorter distance of the channels in PCN-222 NPs than L-PCN-222 MPs also makes it easier for Cyt c to diffuse inside particles. In addition, stirring increased the encapsulation efficiency of Cyt c.

Combined, we loaded Cyt c within PCN-222 NPs through a 3-h incubation under stirring. The obtained Cyt c@PCN-222 NPs exhibited an identical morphology to PCN-222 NPs. The length and width of Cyt c@PCN-222 NPs were measured to be 567 ± 55 nm and 109 ± 13 nm, respectively, which were almost the same as those of PCN-222 NPs (Figure 1c). This proved that PCN-222 NPs remained essentially intact after Cyt c loading. The XRD pattern of Cyt c@PCN-222 NPs also corresponded well with the pattern of simulated PCN-222 (Figure S5). The color of PCN-222 NPs changed from purple to brown after Cyt c encapsulation, which indicated that Cyt c was successfully immobilized (inset photos, Figure 1b and c). Attenuated total reflectance Fourier transform infrared (ATR-FTIR) spectra also proved the successful loading of Cyt c within PCN-222 NPs based on on the amide I band peak at approximately 1650 cm^{-1} (Figure S6). Furthermore, the elemental mappings of Cyt c@PCN-222 NPs showed that elements S and Fe from Cyt c were distributed homogeneously coupled with the element Zr from PCN-222 NPs (Figure 1d), proving that Cyt c was uniformly distributed within PCN-222 NPs. In addition, the N_2 uptake and pore volume of PCN-222 NPs decreased obviously after Cyt c loading (Figure 1e and f). The BET surface areas of PCN-222 NPs and Cyt c@PCN-222 NPs were measured to be 2115 $m^2 g^{-1}$ and 1120 $m^2 g^{-1}$, respectively. The BET results proved that Cyt c was successfully confined within the channels of PCN-222 NPs.

We further compared the loading amount and loading efficiency of Cyt c between PCN-222 NPs with a pore size of around 3.7 nm and other MOF NPs with varying pore sizes. Four other Zr_6-based MOF NPs, including UiO-66 NPs, MOF-808 NPs, PCN-224 NPs, and NU-1000 NPs, were fabricated, and their pore sizes were around 0.6 nm, 1.8 nm, 1.9 nm, and 3.2 nm, respectively (Figure 2a). The SEM images demonstrated that UiO-66 NPs and MOF-808 NPs exhibited an octahedral shape, while PCN-224 NPs and NU-1000 NPs showed a cubic shape and rod-like shape, respectively. The XRD patterns of the four MOF NPs

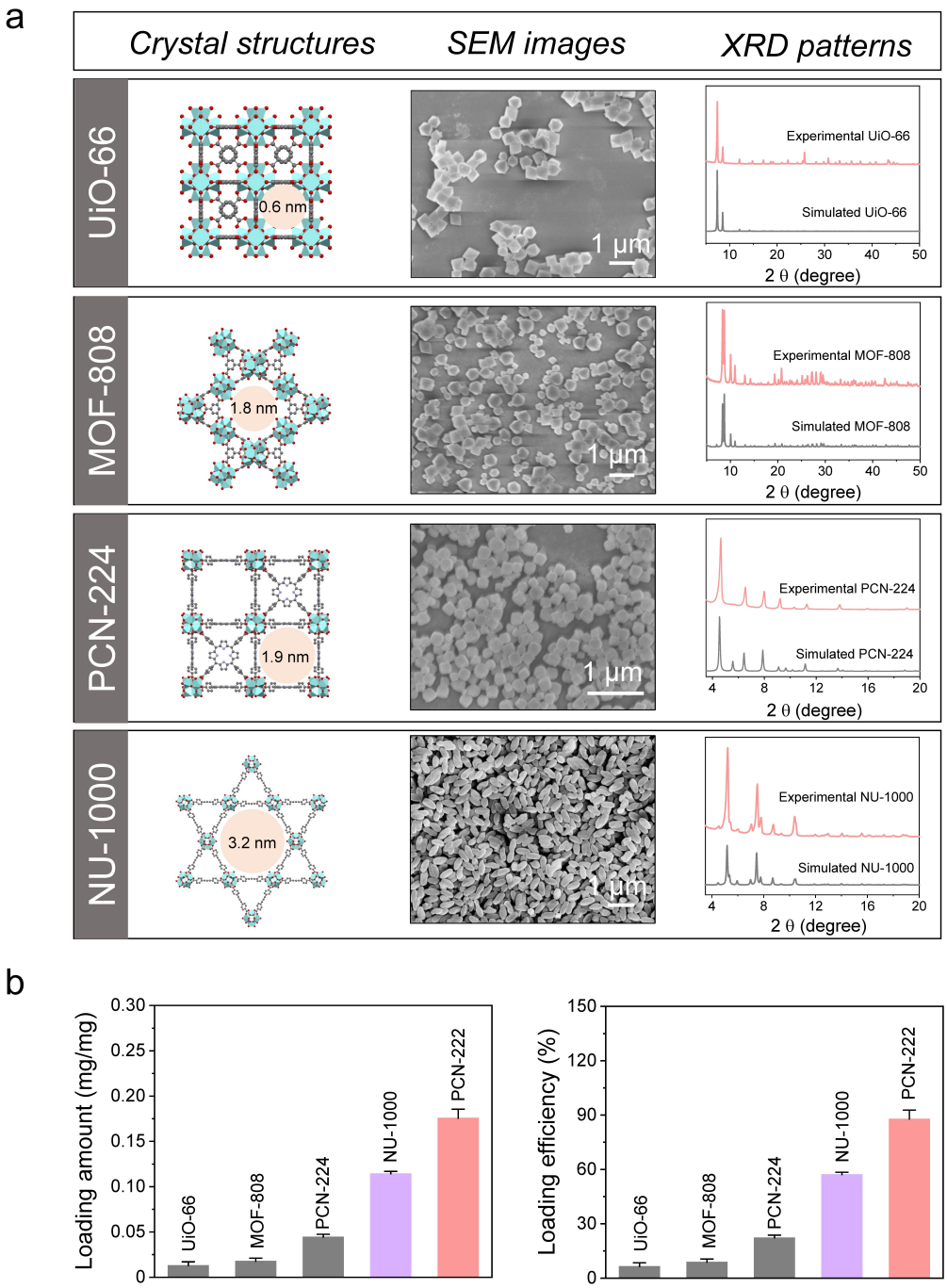

Figure 2. Comparison of Cyt c loading between PCN-222 NPs and other Zr_6-based MOFs. a) Crystal structures, SEM images, and XRD patterns of Zr_6-based MOFs, including UiO-66 NPs, MOF-808 NPs, PCN-224 NPs, and NU-1000 NPs. b) Comparison of Cyt c loading amount and loading efficiency between PCN-222 NPs and other Zr_6-based MOF NPs demonstrated in panel a. Data are expressed as mean ± standard error of 3 experiments.

corresponded well with their simulated counterparts, which indicated the successful synthesis of MOF NPs. To gain an insight into the effect of pore size on Cyt c loading, we employed an identical mass concentration of MOF NPs to encapsulate Cyt c. As shown in Figure 2b, UiO-66 NPs, MOF-808 NPs, and PCN-224 NPs showed limited loading amounts and loading efficiencies of Cyt c compared with PCN-222 NPs. For NU-1000 NPs with a pore size of 3.2 nm, Cyt c can also be confined within NU-1000 NPs. The Cyt c-confined NU-1000 NPs, termed as Cyt c@NU-1000 NPs, showed the identical morphology and XRD pattern to those of NU-1000 NPs (Figures S7 and S8). Though NU-1000 NPs achieved a relatively high loading amount of 114 μg/mg and a loading efficiency of 57 %, it was still lower than the loading amount of 176 μg/mg and the loading efficiency of 88 % achieved by PCN-222 NPs. We further employed the

BCA assay to assess the Cyt c loading within NU-1000 NPs and PCN-222 NPs. As shown in Figure S9, it was confirmed that PCN-222 NPs encapsulated about 50% more Cyt c than NU-1000 NPs. The above results demonstrate the superior performance of PCN-222 NPs in Cyt c loading, which can be ascribed to the large pore size of 3.7 nm. We further monitored the release of Cyt c from Cyt c@PCN-222 NPs during storage. It was shown that Cyt c seldom escaped from the pores in PCN-222 NPs (Figure S10). Cyt c possesses abundant amino groups and carboxyl groups on its surface, which might bind to the PCN-222 scaffold through the electrostatic interaction and coordinative interaction with dangling carboxyl groups and zirconium clusters in PCN-222, respectively. However, the addition of competing reagents against the electrostatic interaction and coordinative interaction, NaCl and sodium acetate (NaAc), hardly influenced the loading amount and release of Cyt c. We therefore speculate that the confinement of Cyt c within the pores in PCN-222 comes from the increased entropy of Cyt c-bound and pore-bound water molecules (Figure S11).[16]

Considering that PCN-222 NPs exhibited a remarkable capacity for Cyt c encapsulation, we measured the peroxidase-like activities of free Cyt c and the confined Cyt c within PCN-222 NPs. Here, we employed a typical peroxidase substrate, 2,2′-azino-bis(3-ethylbenzothiazoline-6-sulfonic acid) diammonium salt (ABTS), the peroxidation product of which is $ABTS^{+\bullet}$ and can be monitored by a UV/VIS spectrophotometer (Figure 3a).[17] We monitored the absorbance changes of ABTS solutions at 728 nm ($A_{728\,nm}$) with the addition of free Cyt c (or confined Cyt c) of an identical concentration in the presence of H_2O_2. The initial velocity of Cyt c@PCN-222 NPs was about 4 folds that of free Cyt c (Figure 3b and c). We also measured the activity of Cyt c@NU-1000 NPs (Figure S12). The result showed that PCN-222 NPs could achieve almost the same activity improvement of Cyt c compared with NU-1000 NPs, while PCN-222 NPs exhibited a much higher Cyt c encapsulation efficiency than NU-1000 NPs. We further monitored the

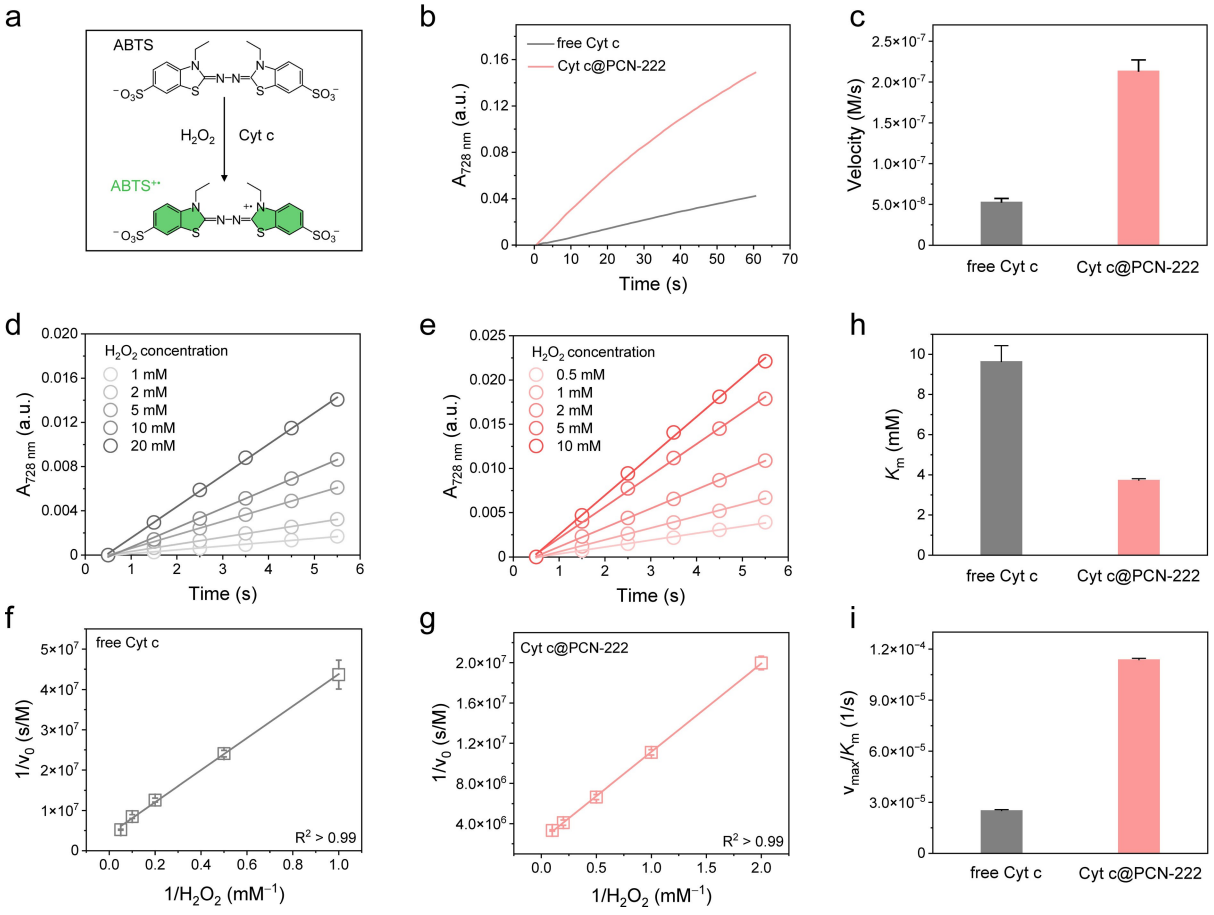

Figure 3. Activity improvement through nanoconfinement and kinetics studies. a) Schematic illustration of ABTS peroxidation catalyzed by Cyt c. b) Time evolution of the absorbance at 728 nm ($A_{728\,nm}$) for monitoring the peroxidase-mimicking catalytic activities of free Cyt c and Cyt c@PCN-222 NPs. The concentrations of Cyt c, H_2O_2, and ABTS were 2.5 μg mL^{-1}, 0.5 mM, and 0.2 mM, respectively. c) The initial velocities corresponding to panel b. d), e) Time evolution of $A_{728\,nm}$ for monitoring the influence of H_2O_2 concentrations on the initial velocities of peroxidation reactions catalyzed by free Cyt c and Cyt c@PCN-222 NPs. The concentrations of Cyt c and ABTS were 0.5 μg mL^{-1} and 0.2 mM, respectively. f), g) Double-reciprocal plots of reciprocal initial velocities versus reciprocal H_2O_2 concentrations corresponding to panels d–e and their linear fittings. h) K_m values and i) v_{max}/K_m values of free Cyt c and PCN-222@Cyt c. Data are expressed as mean ± standard error of 3 experiments.

intrinsic peroxidase-like activity of NU-1000 NPs and PCN-222 NPs. Both MOF NPs showed nearly no activity (Figure S13). This result proved that the activity improvement resulted from the unique nanoconfinement effect rather than the intrinsic activity of MOF NPs. Besides, we did not observe obvious activity decrease in Cyt c induced by the inhibition of substrate diffusion. We speculate that when Cyt c is confined within the 3.7-nm hexagonal pore in PCN-222, the triagonal pore is large enough to guarantee the efficient transport of substrates (Figure S14). Considering the activity enhancement of Cyt c achieved by nanoconfinement, we compared the activity of Cyt c@PCN-222 NPs with that of other nanozymes, including graphene oxide, Fe_3O_4 NPs, NH_2-MIL-88B NPs, and Pt NPs, using an identical mass concentration. The result showed that Cyt c@PCN-222 NPs exhibited higher activity than those nanozymes (Figure S15). Furthermore, the confinement strategy can also effectively improve the storage stability of Cyt c (Figure S16).

To understand the improved peroxidase-mimicking activity through nanoconfinement, we further performed a kinetics study to investigate the difference in the affinity towards H_2O_2 between free Cyt c and the confined Cyt c within PCN-222 NPs. Several concentrations of H_2O_2 were employed in the peroxidation of ABTS catalyzed by free Cyt c and Cyt c@PCN-222 NPs with an identical Cyt c concentration (Figure 3d and e). The obtained initial velocities were further plotted against the corresponding H_2O_2 concentrations in a reciprocal way (Figure 3f and g). The Michaelis constant (K_m) can be obtained based on the linear fitting, which reflects the affinity of an enzyme towards a substrate. As shown in Figure 3h, the K_m values of free Cyt c and Cyt c@PCN-222 NPs were calculated to be 9.6 mM and 3.7 mM, respectively. The much lower K_m value of the confined Cyt c within PCN-222 NPs compared with free Cyt c demonstrated the improved affinity towards H_2O_2 achieved by the nanoconfinement effect. In addition, the maximal velocities (v_{max}) of free Cyt c and the confined Cyt c were also obtained (Figure S17), which showed that the v_{max} of Cyt c was increased but not substantially after confinement. The significant improvement in the activity of Cyt c through nanoconfinement can be mainly ascribed to the increased affinity towards H_2O_2. In combination with K_m and v_{max} values, v_{max}/K_m values, which reflect the catalytic efficiencies of the enzymes, were calculated. As shown in Figure 3i, Cyt c@PCN-222 NPs exhibited an around 4–5 folds higher catalytic efficiency than free Cyt c. This result corresponded well with the measurement of the peroxidase-mimicking activities in Figure 3b.

After having improved the peroxidase-mimicking activity of Cyt c through nanoconfinement for the substrate ABTS, we evaluated the substrate scope by using three other substrates, including 3,3′,5,5′-tetramethylbenzidine (TMB), dopamine, and Amplex Red. The substrate TMB is also widely used for colorimetric assays, and the product $TMB^{+\bullet}$ can be monitored based on its absorbance at 652 nm ($A_{652\,nm}$). As shown in Figure 4a, the confined Cyt c within PCN-222 NPs exhibited much higher activity than free Cyt c. In addition, we also observed an activity improvement for

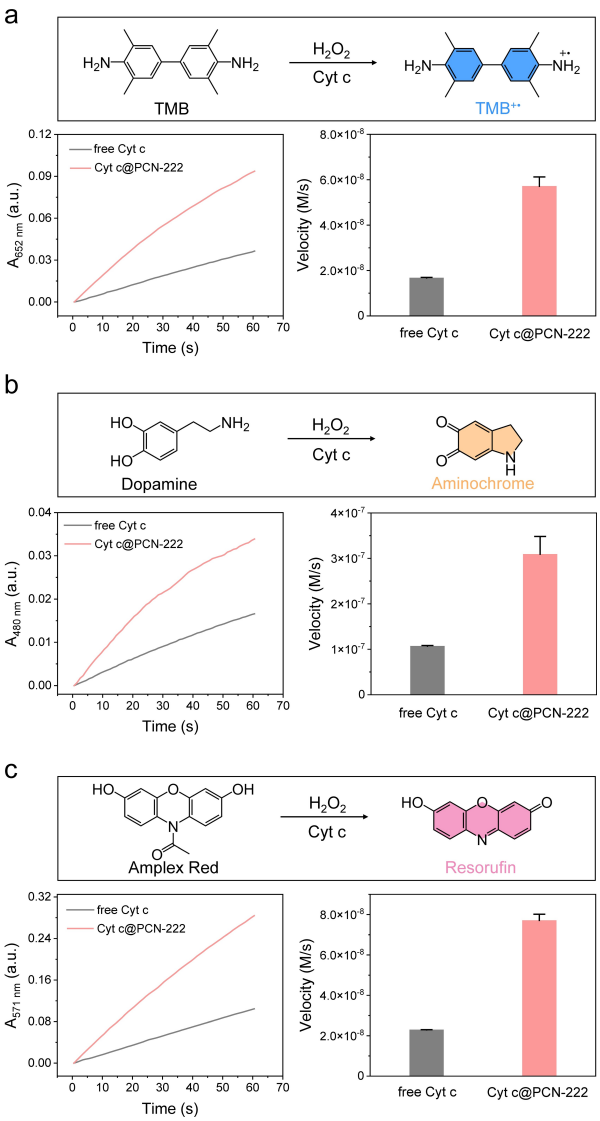

Figure 4. Activity improvement for other substrates. Time evolution of the absorbance at 652 nm ($A_{652\,nm}$), 480 nm ($A_{480\,nm}$), and 571 nm ($A_{571\,nm}$) for monitoring the velocities of peroxidation of a) 0.2 mM TMB, b) 2 mM dopamine, and c) 0.1 mM Amplex red catalyzed by free Cyt c, and Cyt c@PCN-222 NPs in the presence of 0.5 mM H_2O_2, 5 mM H_2O_2, and 0.5 mM H_2O_2, respectively. The concentration of Cyt c was 2.5 $\mu g\,mL^{-1}$. Data are expressed as mean ± standard error of 3 experiments.

the substrate dopamine (Figure 4b). Besides the two substrates mentioned above, we also employed a classic fluorescent substrate, Amplex Red. The peroxidation product, Resorufin, can be monitored by both the absorbance changes and fluorescence changes of the reaction solutions. As shown in Figure 4c and Figure S18, nanoconfinement also enhanced the activity of Cyt c for the substrate Amplex Red.

Ultrasonic cleaners play an essential role in laboratories, which are widely utilized to disperse colloids, dissolve chemicals, fabricate materials, and so on.[18] Recently, some scientists have shown that H_2O_2 can be produced by a commercial ultrasonic humidifier.[19] This might be because

the ultrasonic waves can lead to the formation of a bubble in the liquid, which is called cavitation. When the bubble collapses, it results in high pressures and temperatures, which further promote the formation of H_2O_2 in aqueous solutions.[20] We suppose that a lab-equipped ultrasonic cleaner can also induce the H_2O_2 formation during the operation process, which may impose adverse impacts on our experiments. For example, some chemical bonds, such as phenyl borate esters, are very vulnerable to H_2O_2.[21] Besides, the existence of H_2O_2 may cause defects in materials and deactivation of catalysts.[22] Here, we employed three widely used vessels in labs, including 1.5-mL plastic tubes, 2-mL plastic tubes, and 2-mL glass bottles (Figure 5a). Considering that PCN-222 NPs possess a better Cyt c loading capacity and a comparable improvement in the peroxidase-like activity of Cyt c compared with NU-1000 NPs, we employed Cyt c@PCN-222 NPs to detect the H_2O_2 formation with utilization of the fluorescent substrate, Amplex Red. Horseradish peroxidase (HRP) is a commercial enzyme, which is used for H_2O_2 detection. Compared with HRP, Cyt c@PCN-222 is more stable under harsh conditions (Figure S19). The standard curves of H_2O_2 were

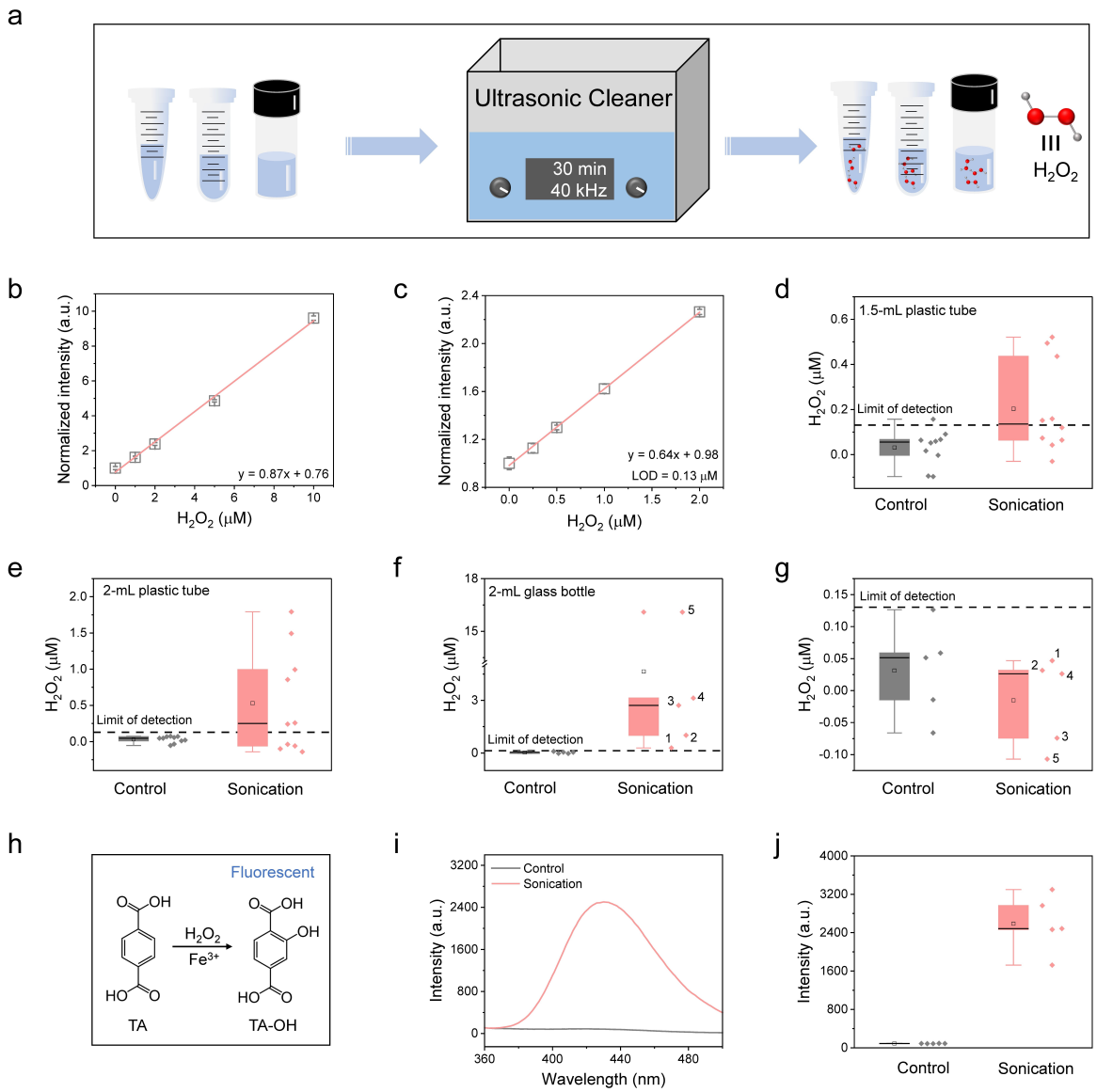

Figure 5. Detection of H_2O_2 formation induced by a lab-equipped ultrasonic cleaner. a) Schematic illustration of H_2O_2 formation in water in different vessels after 30 min of sonication in an ultrasonic cleaner with a frequency of 40 kHz. Linear plots of the normalized intensities of 20 μM Amplex red at 585 nm with λ_{ex} of 560 nm in the presence of Cyt c@PCN-222 NPs and H_2O_2 with varying concentrations ranging from b) 0 μM to 10 μM and c) 0 μM to 2 μM after a 30-min incubation at room temperature. Detection of H_2O_2 formation in water in d) 1.5-mL plastic tubes, e) 2-mL plastic tubes, and f) 2-mL glass bottles using Cyt c@PCN-222/Amplex red assay after 30 min of sonication. g) Detection of H_2O_2 formation corresponding to panel f without Cyt c@PCN-222 NPs. h) Schematic illustration of the TA-OH formation, which is fluorescent, in the presence of H_2O_2 and Fe^{3+} based on the Fenton reaction. i) Fluorescence spectra of TA with λ_{ex} of 315 nm after incubation with Fe^{3+} and water without or with sonication. j) Fluorescence intensities at 425 nm corresponding to panel i.

obtained by employing several known concentrations of H_2O_2. A quite low limit of detection (LOD) of 0.13 μM was achieved by the Cyt c@PCN-222 NPs/Amplex Red assay (Figure 5b and c).

We further monitored the concentrations of H_2O_2 formed in water in 1.5-mL and 2-mL plastic tubes after sonication. We observed that some tubes did contain detectable amounts of H_2O_2, which proved that the lab-quipped ultrasonic cleaner can result in the formation of H_2O_2 (Figure 5d and e). It is noted that not all of the tubes produced detectable H_2O_2. The ultrasonic cleaner in this study contains six distributed ultrasonic transducers underneath the bottom of the equipment. The ultrasonic waves generated from the six transducers may produce complex interferences, leading to large differences in the ultrasonic intensities at different positions (Figure S20). This may result in the difference in H_2O_2 concentrations in different tubes. We also observed the H_2O_2 formation in 2-mL glass bottles using the Cyt c@PCN-222 NPs/Amplex Red assay (Figure 5f). Furthermore, we measured the same samples (labelled as numbers 1–5) without the addition of Cyt c@PCN-222 NPs. As expected, the absence of Cyt c@PCN-222 NPs led to no detection of H_2O_2 formation (Figure 5g). This result ruled out that the potential metal species from the environment can lead to the false positive outcomes. Besides, sonication can lead to an increase in the temperature of the water from room temperature to 44 °C. We also excluded the effect of heating water on the H_2O_2 formation (Figure S21). Furthermore, we employed TA to monitor the H_2O_2 formation based on the Fenton reaction. The iron ions can produce hydroxyl radicals in the presence of H_2O_2, which further react with TA to form TA–OH. TA–OH can be monitored using a fluorescence spectrophotometer (Figure 5h). As shown in Figure 5i and j, the sonication treatment led to significant fluorescence intensities at 425 nm, while no fluorescence was observed without any treatment. This result further proved that the utilization of the lab-equipped ultrasonic cleaner can result in H_2O_2 formation. Besides the ultrasonic cleaner, we also monitored the H_2O_2 formation during the utilization of an ultrasonic probe, which offers researchers a reminder that H_2O_2-sensitive materials may need to avoid sonication treatment (Figure S22).

Conclusion

In summary, we have developed a nanoconfinement strategy to fabricate a protein-confined MOF hybrid nanozyme, Cyt c@PCN-222 NP. Cyt c can be encapsulated within the channels of PCN-222 NPs in a very efficient way. Compared with other MOF NPs, PCN-222 NPs exhibit a higher loading amount and loading efficiency of Cyt c due to the large channel size of 3.7 nm. The confined Cyt c within the channels of PCN-222 NPs exhibits a much higher activity than free Cyt c, which can be ascribed to the improved affinity towards H_2O_2. Furthermore, the Cyt c@PCN-222 NPs have been successfully utilized to detect the formation of H_2O_2 induced by a lab-equipped ultrasonic cleaner with an LOD of 0.13 μM. The detection results suggest that H_2O_2-sensitive materials may need to avoid sonication treatment.

Acknowledgements

This work was funded by the National Key R&D Program of China (2019YFA0709200 and 2021YFF1200700), the National Natural Science Foundation of China (21874067 and 21722503), Jiangsu Provincial Key R&D Program (BE2022836), the PAPD Program, and the Fundamental Research Funds for the Central Universities (021314380195). We thank Mengnan Wu and Prof. Zhaowei Chen for insightful discussion.

Conflict of Interest

The authors declare no conflict of interest.

Data Availability Statement

The data that support the findings of this study are available from the corresponding author upon reasonable request.

Keywords: Cytochrome c · H_2O_2 · Nanoconfinement · Nanozyme · Sonication

[1] a) H. Wei, L. Gao, K. Fan, J. Liu, J. He, X. Qu, S. Dong, E. Wang, X. Yan, *Nano Today* **2021**, *40*, 101269; b) Y. Huang, J. Ren, X. Qu, *Chem. Rev.* **2019**, *119*, 4357–4412; c) R. Zhang, X. Yan, K. Fan, *Acc. Mater. Res.* **2021**, *2*, 534–547.

[2] a) L. Gao, J. Zhuang, L. Nie, J. Zhang, Y. Zhang, N. Gu, T. Wang, J. Feng, D. Yang, S. Perrett, X. Yan, *Nat. Nanotechnol.* **2007**, *2*, 577–583; b) F. Natalio, R. Andre, A. F. Hartog, B. Stoll, K. P. Jochum, R. Wever, W. Tremel, *Nat. Nanotechnol.* **2012**, *7*, 530–535.

[3] a) L. Huang, J. Chen, L. Gan, J. Wang, S. Dong, *Sci. Adv.* **2019**, *5*, eaav5490; b) M. Comotti, C. Della Pina, R. Matarrese, M. Rossi, *Angew. Chem. Int. Ed.* **2004**, *43*, 5812–5815; *Angew. Chem.* **2004**, *116*, 5936–5939; c) Y. Chang, M. Liu, J. Liu, *Anal. Chem.* **2020**, *92*, 3118–3124.

[4] a) T. Wu, S. Huang, H. Yang, N. Ye, L. Tong, G. Chen, Q. Zhou, G. Ouyang, *ACS Mater. Lett.* **2022**, *4*, 751–757; b) N. Singh, S. K. NaveenKumar, M. Geethika, G. Mugesh, *Angew. Chem. Int. Ed.* **2021**, *60*, 3121–3130; *Angew. Chem.* **2021**, *133*, 3158–3167.

[5] a) R. Zhang, L. Chen, Q. Liang, J. Xi, H. Zhao, Y. Jin, X. Gao, X. Yan, L. Gao, K. Fan, *Nano Today* **2021**, *41*, 101317; b) N. Losada-Garcia, A. Jimenez-Alesanco, A. Velazquez-Campoy, O. Abian, J. M. Palomo, *ACS Appl. Mater. Interfaces* **2021**, *13*, 5111–5124.

[6] a) J. E. Mondloch, M. J. Katz, W. C. Isley III, P. Ghosh, P. Liao, W. Bury, G. W. Wagner, M. G. Hall, J. B. DeCoste, G. W. Peterson, R. Q. Snurr, C. J. Cramer, J. T. Hupp, O. K. Farha, *Nat. Mater.* **2015**, *14*, 512–516; b) H. G. T. Ly, G. Fu, A. Kondinski, B. Bueken, D. De Vos, T. N. Parac-Vogt, *J. Am. Chem. Soc.* **2018**, *140*, 6325–6335; c) R. Walther, A. K. Winther, A. S. Fruergaard, W. van den Akker, L. Sorensen, S. M.

Nielsen, M. T. Jarlstad Olesen, Y. Dai, H. S. Jeppesen, P. Lamagni, A. Savateev, S. L. Pedersen, C. K. Frich, C. Vigier-Carriere, N. Lock, M. Singh, V. Bansal, R. L. Meyer, A. N. Zelikin, *Angew. Chem. Int. Ed.* **2019**, *58*, 278–282; *Angew. Chem.* **2019**, *131*, 284–288; d) S. Neri, S. Garcia Martin, C. Pezzato, L. J. Prins, *J. Am. Chem. Soc.* **2017**, *139*, 1794–1797.

[7] a) L. Jiao, W. Xu, H. Yan, Y. Wu, C. Liu, D. Du, Y. Lin, C. Zhu, *Anal. Chem.* **2019**, *91*, 11994–11999; b) Z. Xi, K. Wei, Q. Wang, M. J. Kim, S. Sun, V. Fung, X. Xia, *J. Am. Chem. Soc.* **2021**, *143*, 2660–2664; c) Z. Farka, V. Cunderlova, V. Horackova, M. Pastucha, Z. Mikusova, A. Hlavacek, P. Skladal, *Anal. Chem.* **2018**, *90*, 2348–2354; d) D. Liu, C. Ju, C. Han, R. Shi, X. Chen, D. Duan, J. Yan, X. Yan, *Biosens. Bioelectron.* **2021**, *173*, 112817; e) X. Wang, L. Qin, M. Zhou, Z. Lou, H. Wei, *Anal. Chem.* **2018**, *90*, 11696–11702; f) M. Broto, M. M. Kaminski, C. Adrianus, N. Kim, R. Greensmith, S. Dissanayake-Perera, A. J. Schubert, X. Tan, H. Kim, A. S. Dighe, J. J. Collins, M. M. Stevens, *Nat. Nanotechnol.* **2022**, *17*, 1120–1126.

[8] J. R. Sanchez-Valencia, T. Dienel, O. Groning, I. Shorubalko, A. Mueller, M. Jansen, K. Amsharov, P. Ruffieux, R. Fasel, *Nature* **2014**, *512*, 61–64.

[9] U. Olsbye, S. Svelle, M. Bjorgen, P. Beato, T. V. Janssens, F. Joensen, S. Bordiga, K. P. Lillerud, *Angew. Chem. Int. Ed.* **2012**, *51*, 5810–5831; *Angew. Chem.* **2012**, *124*, 5910–5933.

[10] H. Furukawa, K. E. Cordova, M. O'Keeffe, O. M. Yaghi, *Science* **2013**, *341*, 1230444.

[11] A. B. Grommet, M. Feller, R. Klajn, *Nat. Nanotechnol.* **2020**, *15*, 256–271.

[12] a) X. Lian, Y. Fang, E. Joseph, Q. Wang, J. Li, S. Banerjee, C. Lollar, X. Wang, H. C. Zhou, *Chem. Soc. Rev.* **2017**, *46*, 3386–3401; b) Y. Chen, V. Lykourinou, C. Vetromile, T. Hoang, L. J. Ming, R. W. Larsen, S. Ma, *J. Am. Chem. Soc.* **2012**, *134*, 13188–13191.

[13] a) Y. Chen, F. Jimenez-Angeles, B. Qiao, M. D. Krzyaniak, F. Sha, S. Kato, X. Gong, C. T. Buru, Z. Chen, X. Zhang, N. C. Gianneschi, M. R. Wasielewski, M. Olvera de la Cruz, O. K. Farha, *J. Am. Chem. Soc.* **2020**, *142*, 18576–18582; b) W.-H. Chen, M. Vázquez-González, A. Zoabi, R. Abu-Reziq, I. Willner, *Nat. Catal.* **2018**, *1*, 689–695; c) F. S. Liao, W. S. Lo, Y. S. Hsu, C. C. Wu, S. C. Wang, F. K. Shieh, J. V. Morabito, L. Y. Chou, K. C. Wu, C. K. Tsung, *J. Am. Chem. Soc.* **2017**, *139*, 6530–6533; d) F. Lyu, Y. Zhang, R. N. Zare, J. Ge, Z. Liu, *Nano Lett.* **2014**, *14*, 5761–5765; e) C. Xing, P. Mei, Z. Mu, B. Li, X. Feng, Y. Zhang, B. Wang, *Angew. Chem. Int. Ed.* **2022**, *61*, e202201378; *Angew. Chem.* **2022**, *134*, e202201378.

[14] D. Feng, Z. Y. Gu, J. R. Li, H. L. Jiang, Z. Wei, H. C. Zhou, *Angew. Chem. Int. Ed.* **2012**, *51*, 10307–10310; *Angew. Chem.* **2012**, *124*, 10453–10456.

[15] S. Wang, Y. Chen, S. Wang, P. Li, C. A. Mirkin, O. K. Farha, *J. Am. Chem. Soc.* **2019**, *141*, 2215–2219.

[16] T. Y. Tai, F. Sha, X. Wang, X. Wang, K. Ma, K. O. Kirlikovali, S. Su, T. Islamoglu, S. Kato, O. K. Farha, *Angew. Chem. Int. Ed.* **2022**, *61*, e202209110; *Angew. Chem.* **2022**, *134*, e202209110.

[17] S. H. Wen, X. L. Zhong, Y. D. Wu, R. P. Liang, L. Zhang, J. D. Qiu, *Anal. Chem.* **2019**, *91*, 6487–6497.

[18] a) J. Xu, Y. Wang, H. Shan, Y. Lin, Q. Chen, V. A. Roy, Z. Xu, *ACS Appl. Mater. Interfaces* **2016**, *8*, 18991–18997; b) Z. Huang, F.-W. Yan, G.-Q. Yuan, *ACS Sustainable Chem. Eng.* **2018**, *6*, 3187–3195.

[19] N. H. Musskopf, A. Gallo, Jr., P. Zhang, J. Petry, H. Mishra, *J. Phys. Chem. Lett.* **2021**, *12*, 11422–11429.

[20] a) K. S. Suslick, *Science* **1990**, *247*, 1439–1445; b) P. Riesz, D. Berdahl, C. L. Christman, *Environ. Health Perspect.* **1985**, *64*, 233–252.

[21] Y. Liu, Y. Liu, J. Zang, A. A. I. Abdullah, Y. Li, H. Dong, *ACS Biomater. Sci. Eng.* **2020**, *6*, 6510–6527.

[22] a) G. Bae, M. W. Chung, S. G. Ji, F. Jaouen, C. H. Choi, *ACS Catal.* **2020**, *10*, 8485–8495; b) C. C. Pavel, S.-H. Park, A. Dreier, B. Tesche, W. Schmidt, *Chem. Mater.* **2006**, *18*, 3813–3820.

Manuscript received: August 23, 2022
Accepted manuscript online: January 27, 2023
Version of record online: February 8, 2023